

Electronic Supplementary Material

**Hierarchical FeCo LDH/NiSe heterostructure
electrocatalysts with rich heterointerfaces for robust water
splitting at industrial-level current density**

Weiwei Han,^{†,‡} Wenyi Wang,[†] Jiahong Liao,[†] Yi He,^{†,‡} Xingwang Zhang,^{,†} Chunlin Yu^{*,†,‡}*

[†] Institute of Zhejiang University-Quzhou, Quzhou 324000, China

[‡] College of Chemical and Biological Engineering, Zhejiang University, Hangzhou 310027, China

*Corresponding authors

E-mail: xwzhang@zju.edu.cn (Xingwang Zhang), chunlinyu@zju.edu.cn (Chunlin Yu)

Supplementary Experimental Details

1. Electrochemical active surface area (ECSA) calculation: The ECSA can be estimated from the double layer capacitances (C_{dl}) by the equation.

$$ECSA = \frac{C_{dl}}{C_s} \times A \quad (1)$$

Where the C_s of $40 \mu\text{F cm}^{-2}$ is the specific capacitance for the flat surface, and A is the geometric surface area of the electrode (0.4 cm^2).

2. Faradaic efficiency (FE) calculation: The FE was calculated by comparing the actual amount of O_2 production with the theoretical amount of O_2 .

$$FE\% = \frac{4 \times 96485 \times n}{I \times t} \times 100\% \quad (2)$$

In the equation, n (mol) is the amount of O_2 measured from the corresponding volume, I is the current (A), t is the measured time (s).

3. Mass activity (MA) calculation: The MA (A g^{-1}) of catalysts was calculated by the following equation :

$$MA = \frac{j}{m} \quad (4)$$

Where j is the measured current density, m is the catalyst loading.

4. Computational methods

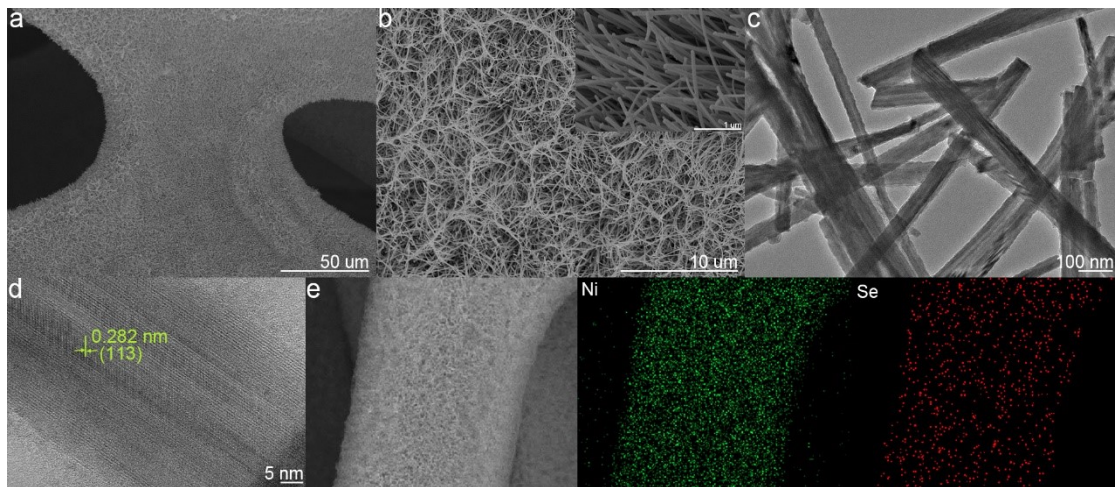


Figure S1. (a) Low- and (b) high-magnification SEM images, (c, d) TEM and HRTEM images, and (d) corresponding EDS elemental mapping images of NiSe@NF.

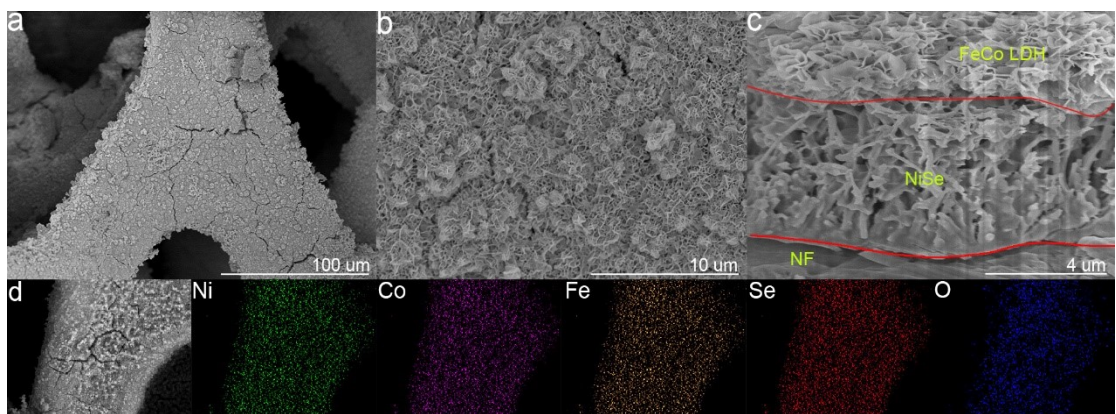


Figure S2. (a) Low- and (b, c) high-magnification SEM images, and (d) EDS elemental mapping images of FeCo LDH/NiSe@NF.

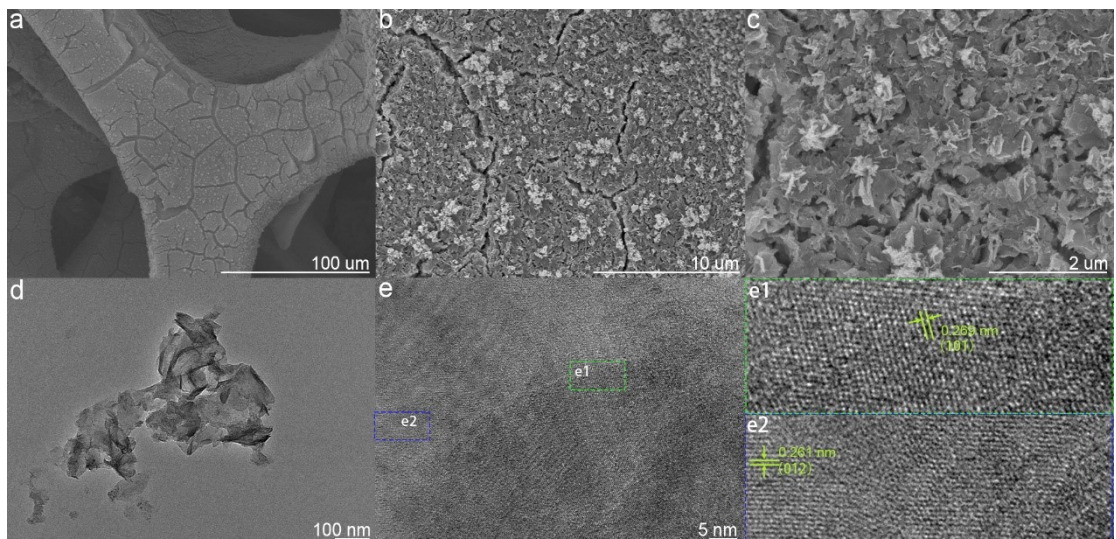


Figure S3. (a) Low- and (b, c) high-magnification SEM images, (d) TEM image, and (e) HRTEM images and (e1, e2) the lattice fringe images of the squared part of FeCo LDH@NF.

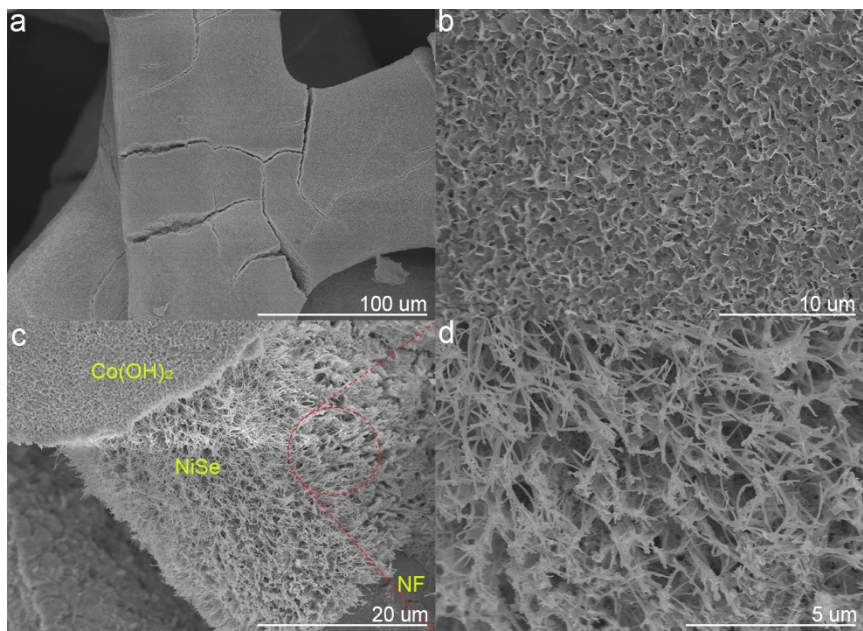


Figure S4. (a) Low- and (b-d) high-magnification SEM images of Co(OH)₂/NiSe@NF.

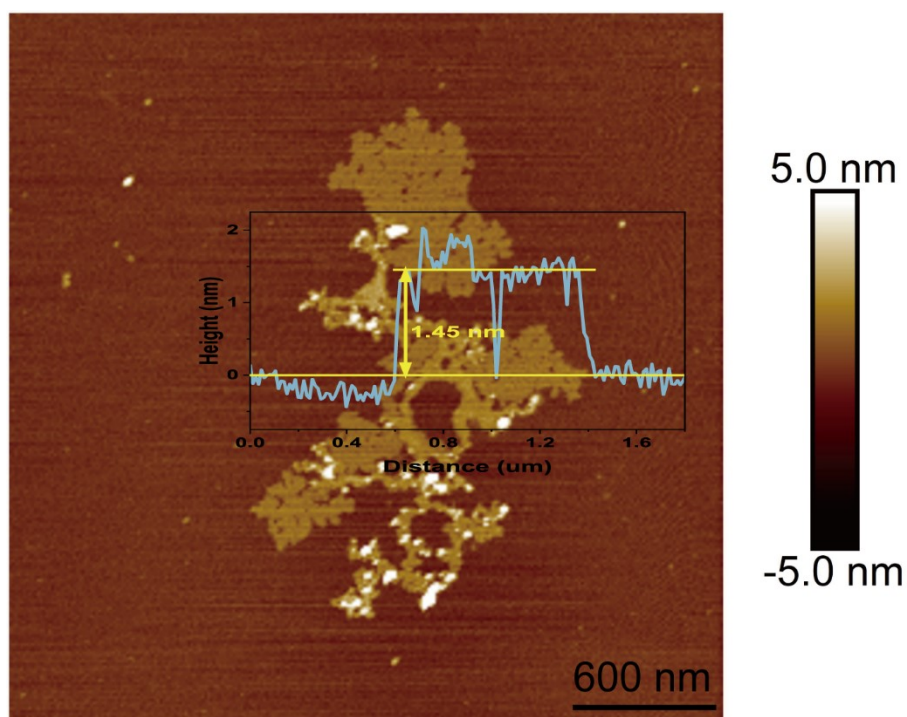


Figure S5. The AFM image and the corresponding AFM height profile (inset) of FeCo LDH.

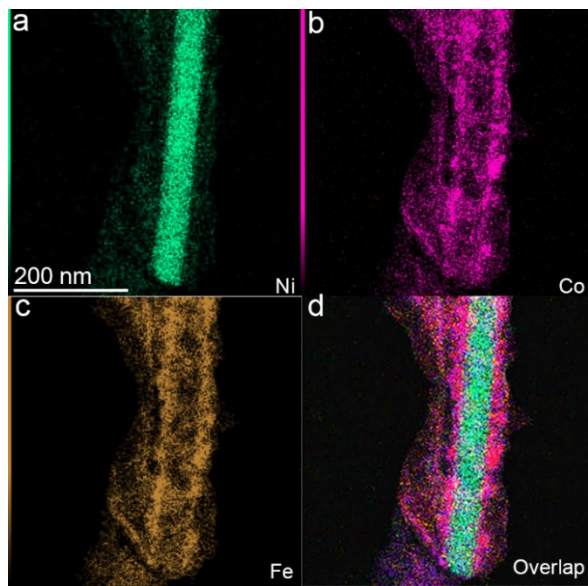


Figure S6. EDS mapping images of FeCo LDH/NiSe@NF: (a) Ni, (b) Co, (c) Fe, and (d) Ni + Co + Fe overlap.

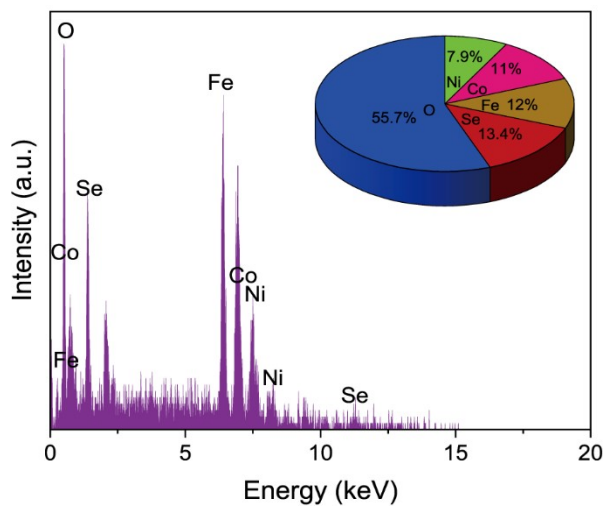


Figure S7. EDS profile of FeCo LDH/NiSe@NF.

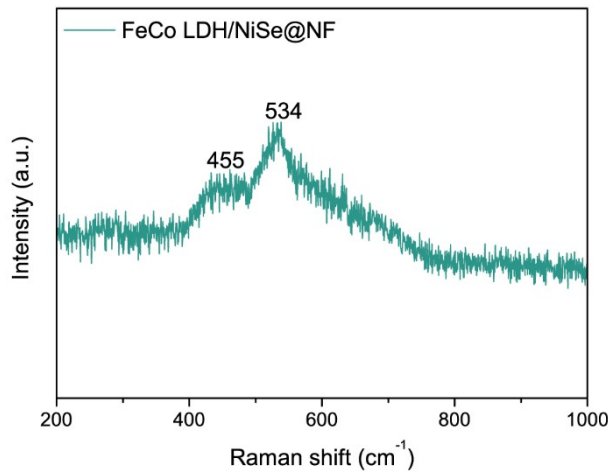


Figure S8. Raman spectrum of FeCo LDH/NiSe@NF.

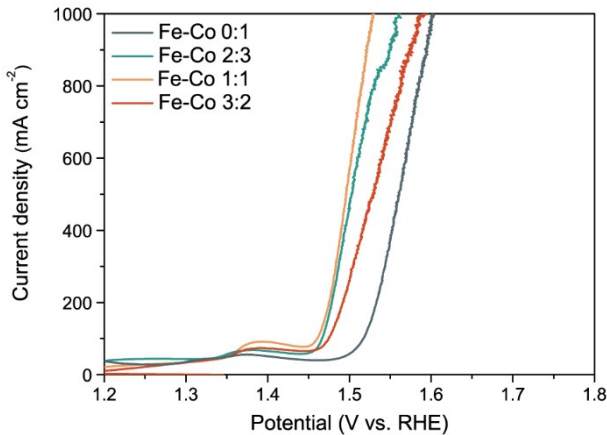


Figure S9. The LSV polarization curves of FeCo LDH/NiSe@NF with different molar ratios of pristine $\text{FeSO}_4 \cdot 7\text{H}_2\text{O}$ and $\text{Co}(\text{NO}_3)_2 \cdot 6\text{H}_2\text{O}$.

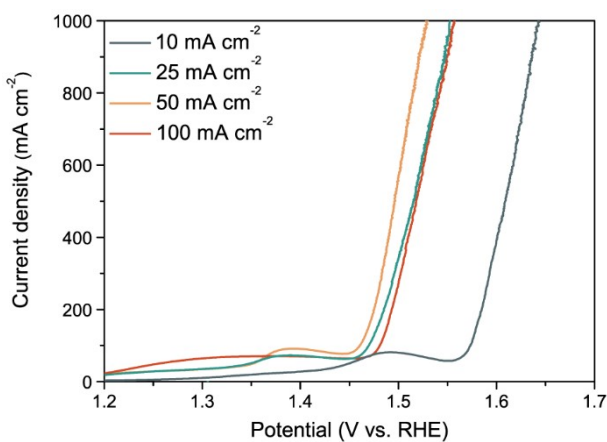


Figure S10. The LSV polarization curves of FeCo LDH/NiSe@NF obtained under different electrodeposition current densities.

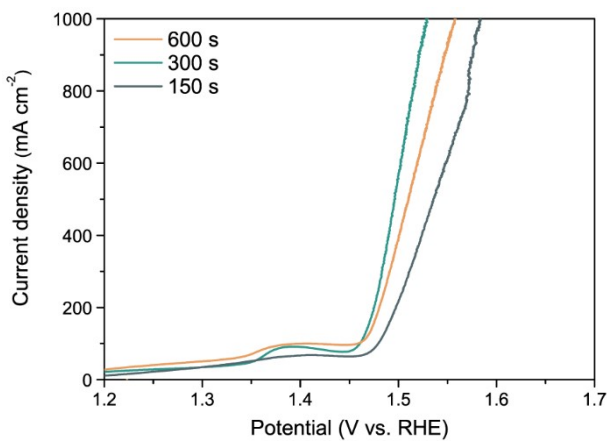


Figure S11. The LSV polarization curves of FeCo LDH/NiSe@NF obtained under different electrodeposition time.

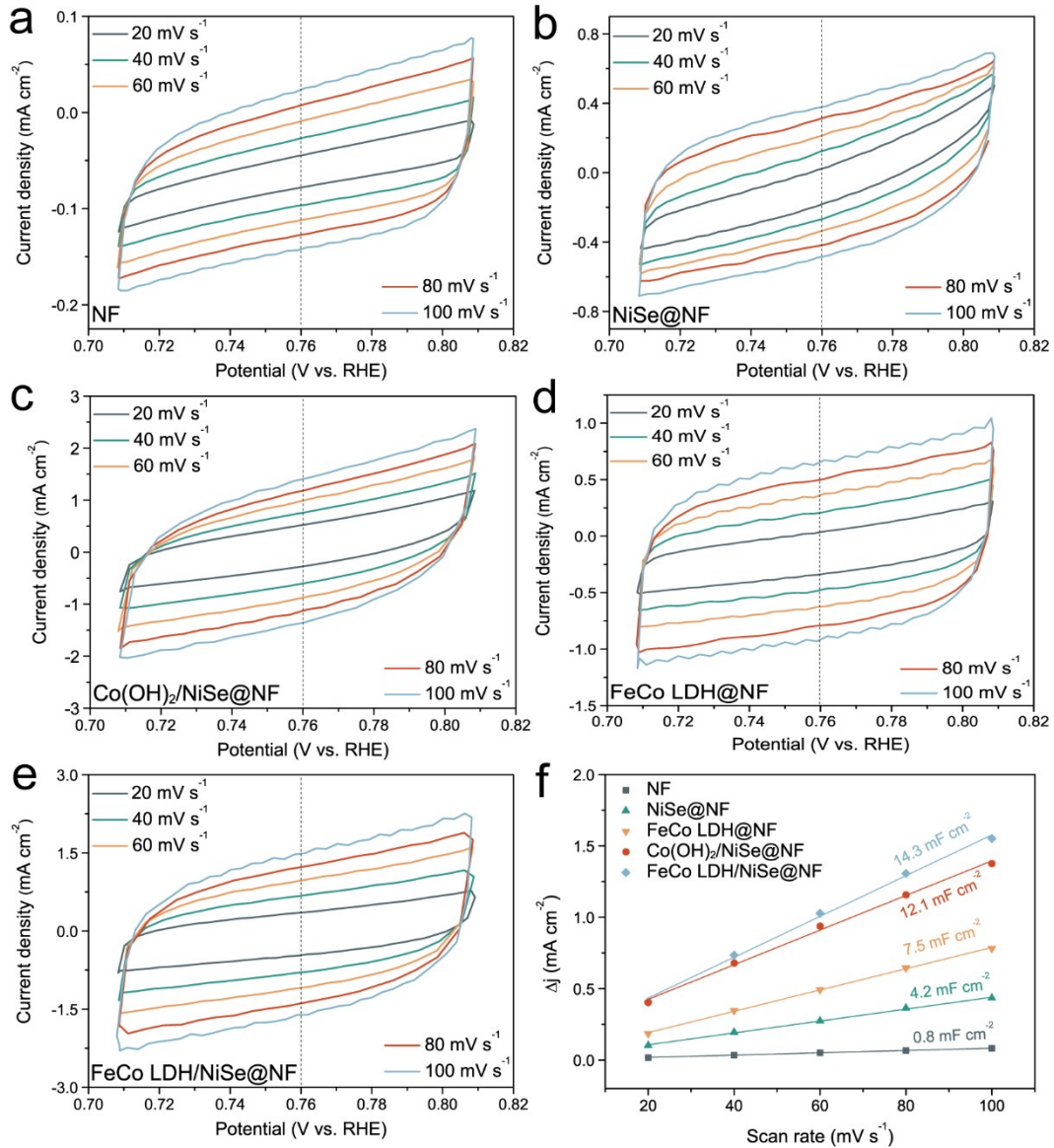


Figure S12. CV curves of (a) NF, (b) NiSe@NF, (c) Co(OH)₂/NiSe@NF, (d) FeCo LDH@NF, and (e) FeCo LDH/NiSe@NF at different scan rates from 20 to 100 mV s⁻¹. (f) Corresponding C_{dl} plots of the above samples.

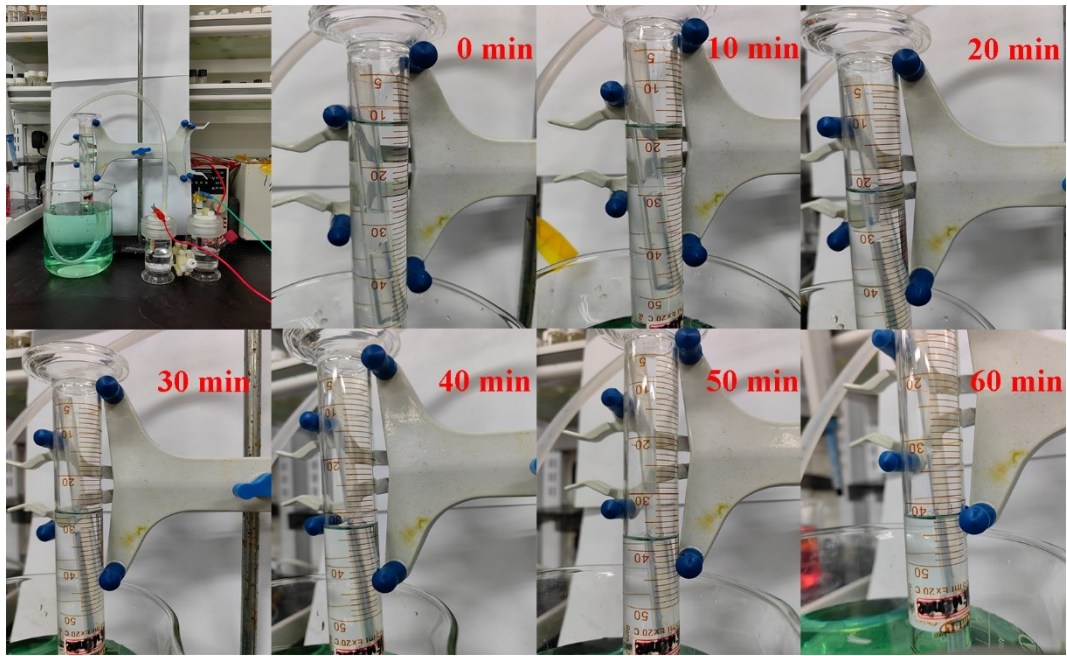


Figure S13. Optical photos of O_2 collection set-up and O_2 volume readings taken every ten minutes for Faradic efficiency measurement.

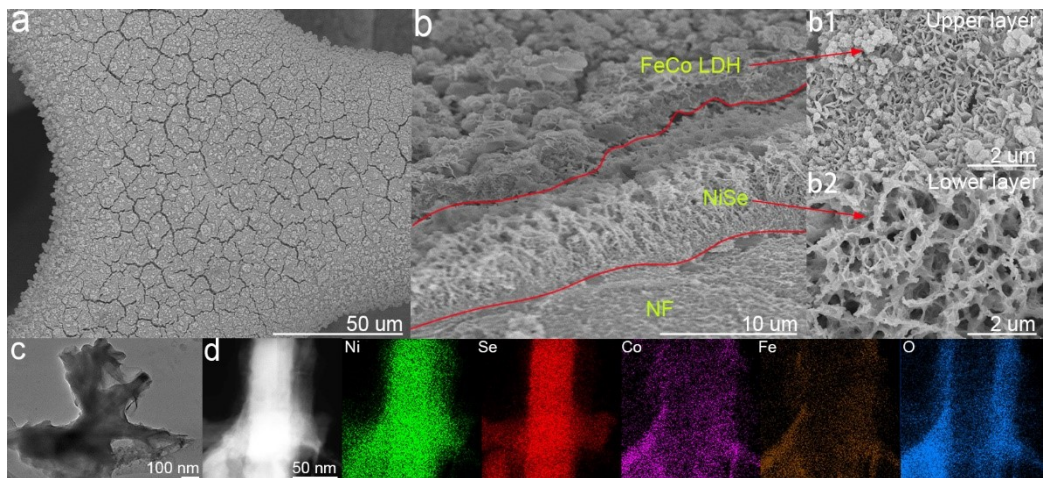


Figure S14. (a) Low- and (b) high-magnification SEM images, (c) TEM image, (d) HAADF-STEM and corresponding elemental mapping images of FeCo LDH/NiSe@NF after OER stability test.

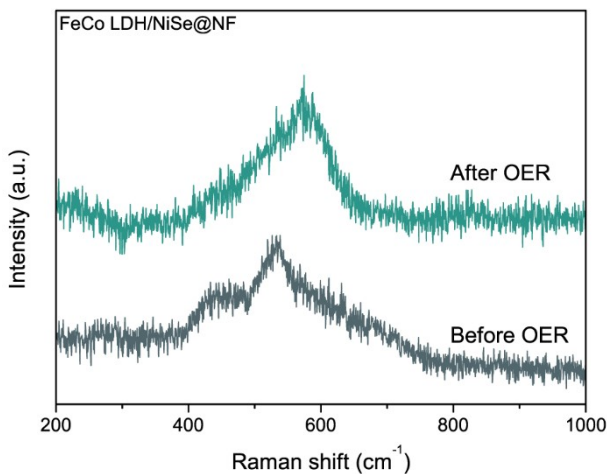


Figure S15. Raman spectra of FeCo LDH/NiSe@NF before and after OER stability test.

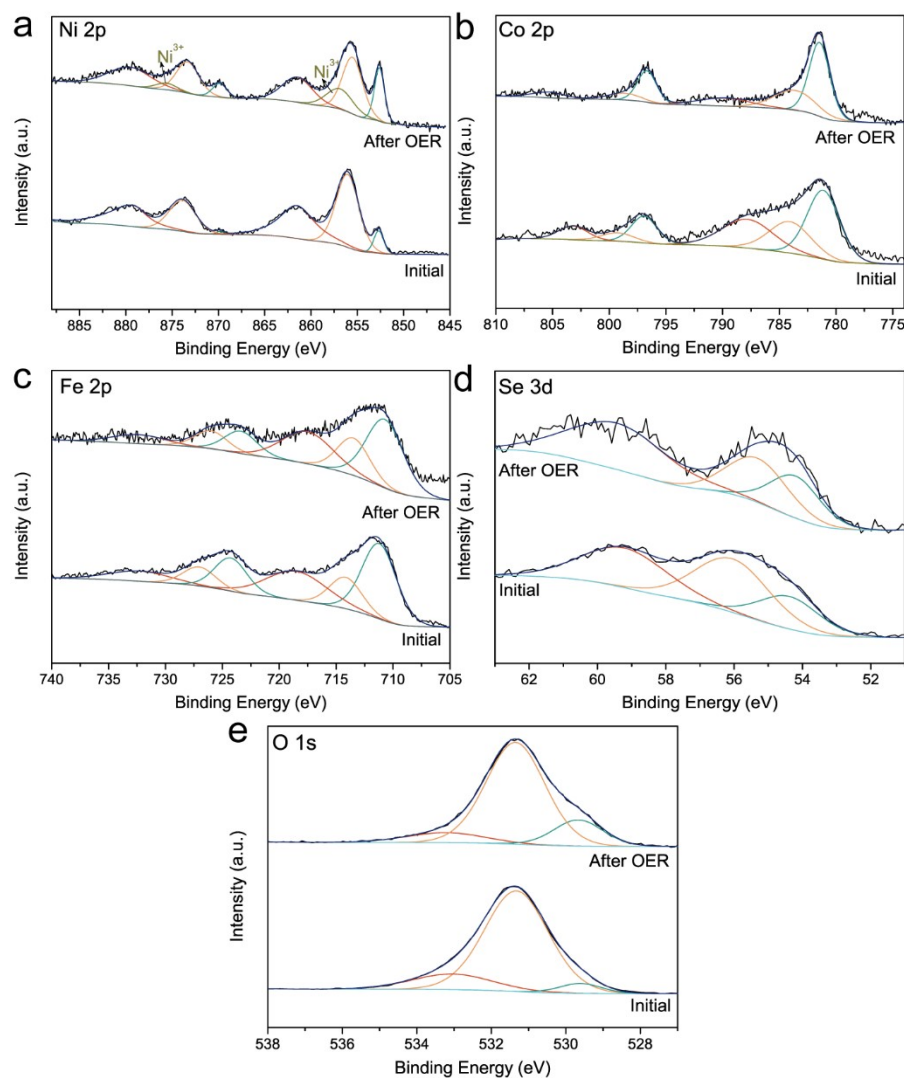


Figure S16. High-resolution XPS spectra of (a)Ni 2p, (b) Co 2p, (c) Fe 2p, (d) Se 3d, and (e) O 1s for FeCo LDH/NiSe@NF before and after OER stability test.

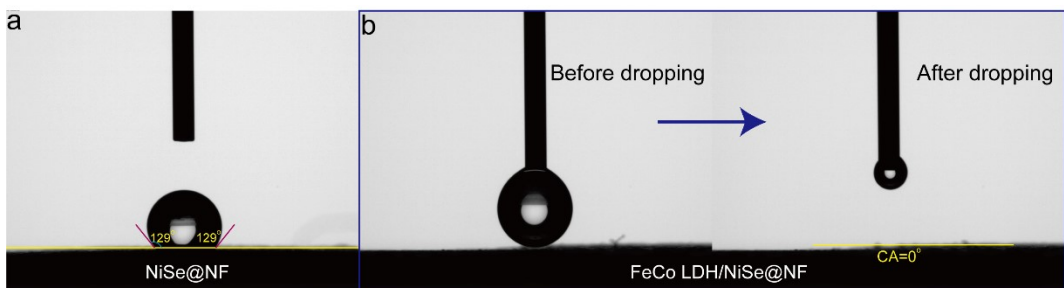


Figure S17. Contact angles of (a) NiSe@NF and (b) FeCo LDH/NiSe@NF.

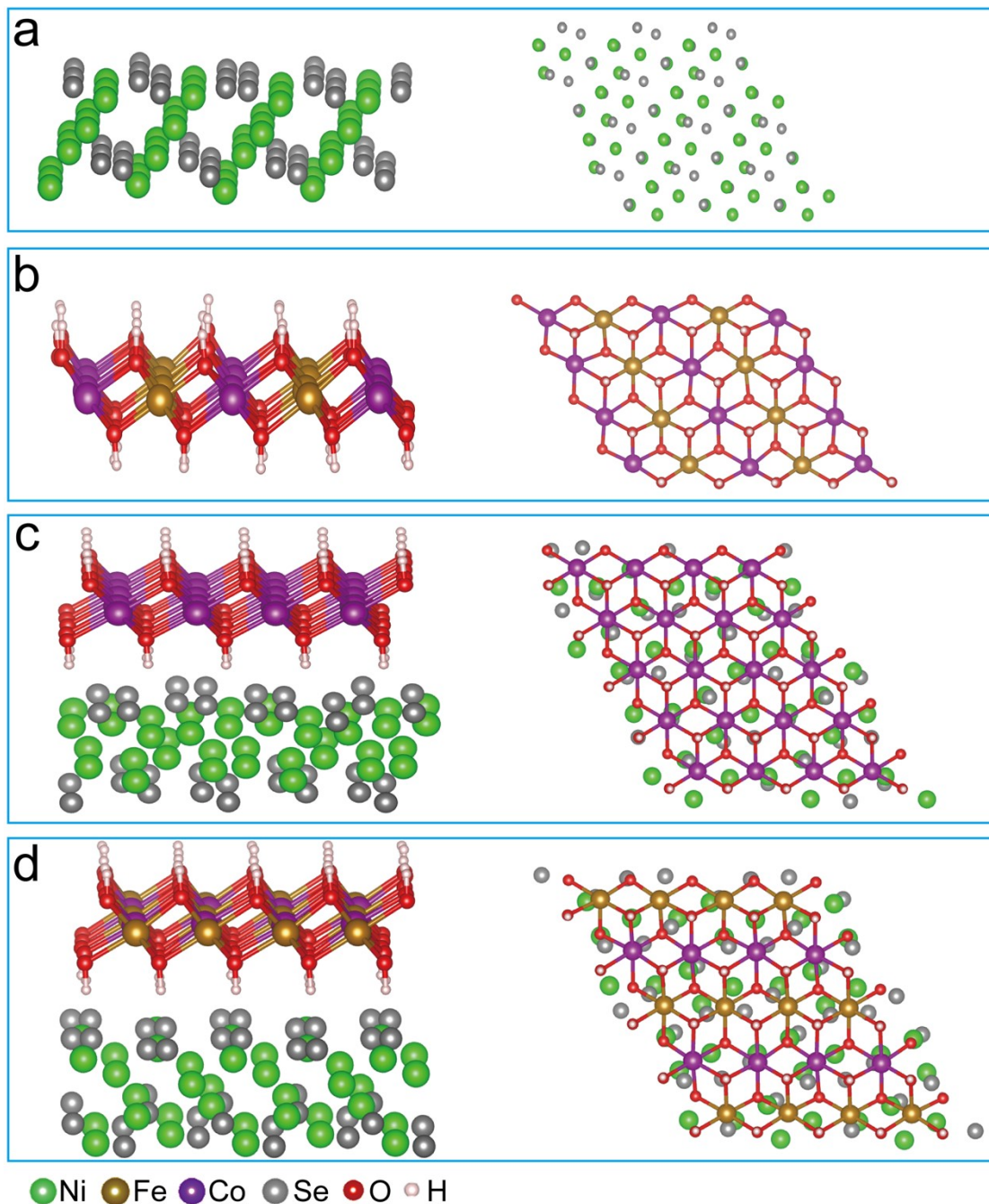


Figure S18. Structure models of (a) NiSe, (b) FeCo LDH, (c) Co(OH)₂/NiSe, and (d) FeCo LDH/NiSe.

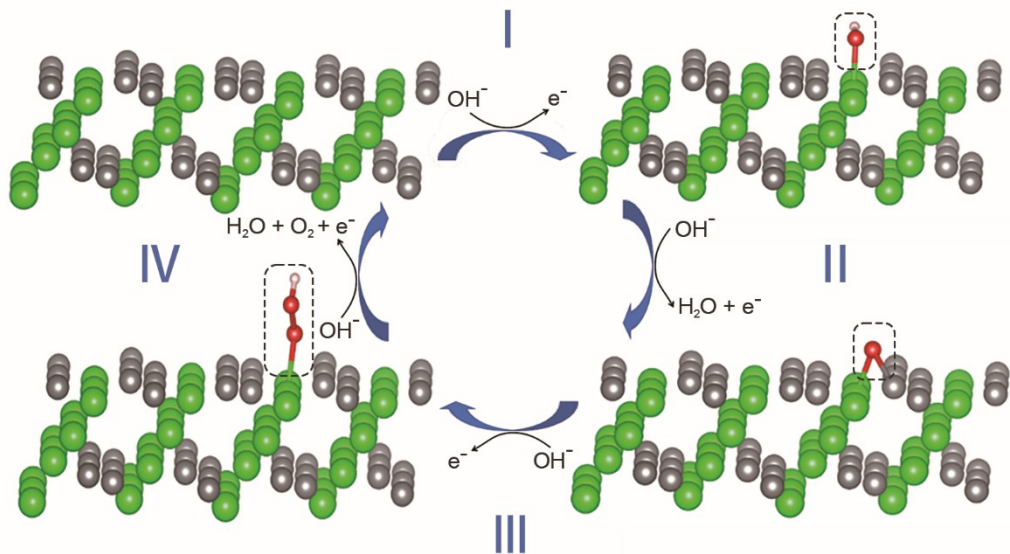


Figure S19. Four electrons reaction process over optimized structure models with oxygen intermediates ($^*\text{OH}$, $^*\text{O}$, and $^*\text{OOH}$) adsorbed on the surface active sites of NiSe for alkaline OER.

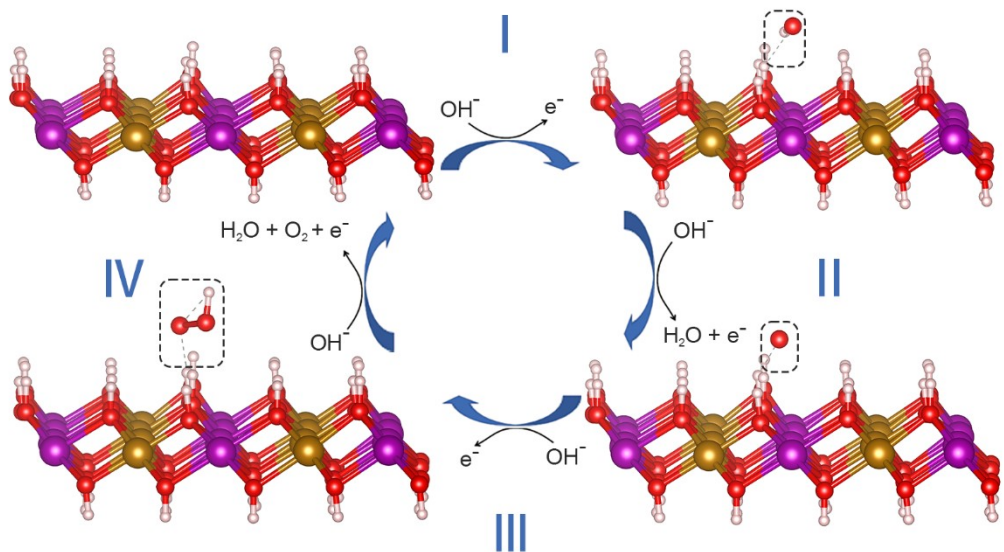


Figure S20. Four electrons reaction process over optimized structure models with oxygen intermediates ($^*\text{OH}$, $^*\text{O}$, and $^*\text{OOH}$) adsorbed on the surface active sites of FeCo LDH for alkaline OER.

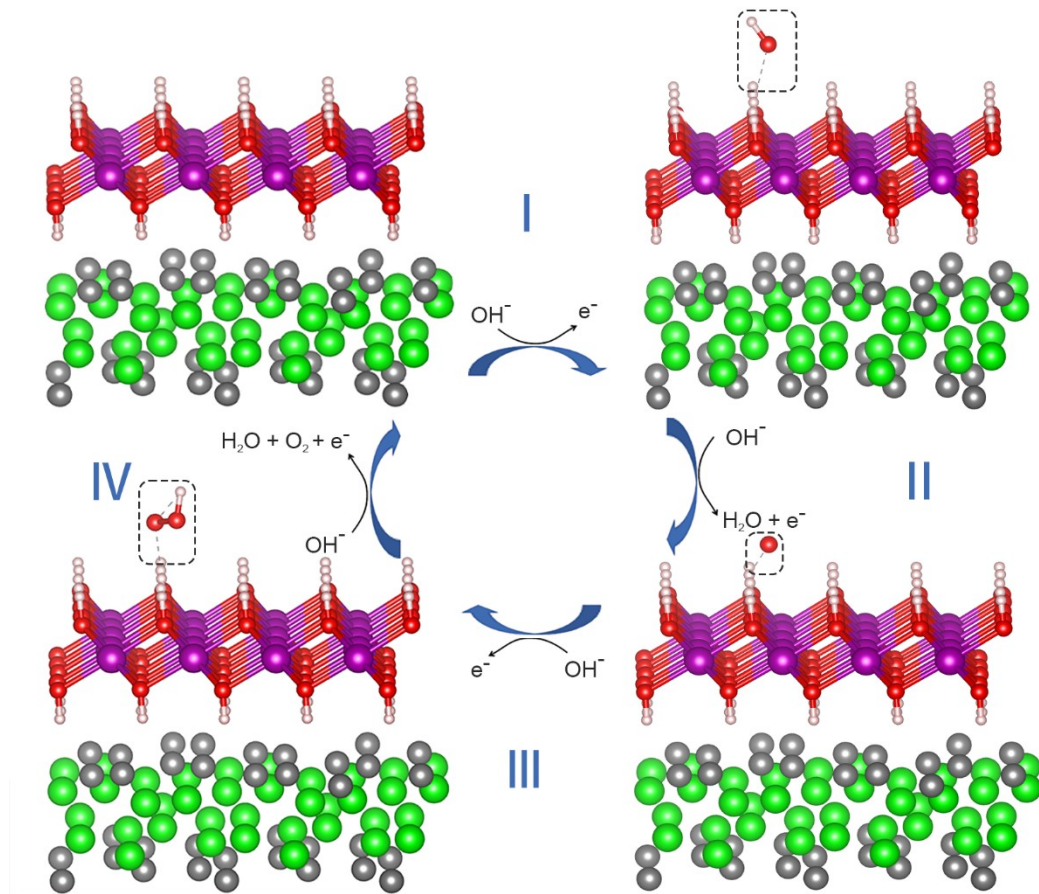


Figure S21. Four electrons reaction process over optimized structure models with oxygen intermediates ($*\text{OH}$, $*\text{O}$, and $*\text{OOH}$) adsorbed on the surface active sites of $\text{Co}(\text{OH})_2/\text{NiSe}$ for alkaline OER.

Table S1. The elemental molar content (at%) of different catalysts determined by EDS.

Elements	NiSe@NF	FeCo LDH/NiSe@NF	FeCo LDH/NiSe@NF (post-OER)
Ni	42.40	7.90	8.17
Co	—	11.03	13.95
Fe	—	11.95	15.61
Se	57.60	13.41	8.27
O	—	55.71	54.00

Table S2. Comparison of the OER performance of the FeCo LDH/NiSe@NF with other recently reported electrocatalysts in 1.0 M KOH.

Catalyst	Substrate	η_{100} (mV)	η_{500} (mV)	η_{1000} (mV)	Stability	Reference
FeCo LDH/NiSe	Nickel foam	230	266	298	t₁₀₀₀=100 h	This work
Cu@NiFe LDH	Cu foam	281	311	315	t ₁₀₀ =48 h	[1]
(Ni,Fe)OOH	Nickel foam	—	259	289	t ₁₀₀₀ =48 h	[2]
NiFe LDH/NiS	Nickel foam	277	—	325	t ₄₀₀ =100 h	[3]
R-NiFeO _x H _y	Nickel foam	266	302	313	t ₅₀₀ =500 h	[4]
Fe ₂ O ₃ @Ni ₂ P/Ni(PO ₃) ₂	Nickel foam	300	340	370	t ₁₀₀₀ =8 h	[5]
FeP/Ni ₂ P	Nickel foam	—	280	293	t ₁₀₀ =25 h	[6]
S-doped FeOOH	Iron foam	~290	324	358	t ₁₀₀₀ =1000 h	[7]
FeOOH-CoS/NF	Nickel foam	~260	306	329	t ₅₀₀ =50 h	[8]
Zn-Fe _x Ni _(1-x) OOH	Nickel foam	269	310	330	t ₁₀₀₀ =1000 h	[9]
MnCo/NiSe	Nickel foam	—	340.4	370.7	t ₅₀₀ =200 h	[10]
CoNi-LDH/Fe MOF	Nickel foam	235	275	305	t ₅₀₀ =40 h	[11]
Ni/MoO ₂ @CN	Nickel foam	~310	~380	420	t ₁₀₀₀ =200 h	[12]
NiCo@C-NiCoMoO	Nickel foam	—	370	390	t ₁₀₀₀ =340 h	[13]
Fe MOF-Ni ₃ S ₂	Nickel foam	243	283	309	t ₅₀₀ =20 h	[14]
Mn _{0.15} -NiFe LDH/Fe _{0.64} Ni _{0.36}	Nickel mesh	242	295	345	t ₅₀₀ =250 h	[15]
Ru ₁ SACs@FeCo-LDH	Nickel foam	—	230	246	t ₁₀₀₀ =1200 h	[16]
Ni ₂ P-Fe ₂ P	Nickel foam	261	~310	337	t ₅₀₀ =48 h	[17]
FeNiOOH(Se)/IF	Iron foam	279	348	—	t ₁₀₀ =100 h	[18]

Note: The summarized stability tests were performed at 100, 500 or 1000 mA cm⁻².

Table S3. Comparison of the overall water splitting performance for the NiCoP/NiCoS_x@NF||FeCo LDH/NiSe@NF with other reported electrocatalysts in 1.0 M KOH.

Electrode	Cell voltage (V) @100 mA cm ⁻²	Stability (h)	Reference
NiCoP/NiCoS_x@NF FeCo LDH/NiSe@NF	1.718	200@500 mA cm⁻²	This work
Fe ₂ O ₃ @Ni ₂ P/Ni(PO ₃) ₂ /NF	1.93	10@3.0 V	[19]
Mo-Ni ₃ S ₂ /Ni _x P _y	~1.79	72@1.85 V	[20]
NiCoP@Co _{0.5} Ni _{0.5} Se ₂ /NF NiFe- LDH/NF	1.75	100@500 mA cm ⁻²	[21]
Fe _{7.4%} -NiSe	1.74	27@1.634 V	[22]
CoP NFs	~1.91	30@1.7 V	[23]
Cr _{0.05} Ni _{0.95} Se ₂ /CC	~1.89	24@10 mA cm ⁻²	[24]
MnCoP/NF	1.97	240@100 mA cm ⁻²	[25]
Mn-doped Ni ₂ O ₃ /Ni ₂ P//Mn- doped Ni _x S _y /Ni ₂ P	~1.73	120@50 mA cm ⁻²	[26]
CoMoS _x /NF	1.74	100@500 mA cm ⁻²	[27]

Table S4. Bader charge analysis of NiSe.

Element	Atom number	Quantity of charge	Change of charges
		(e)	(e)
Ni	1	9.7505	-0.2495
Ni	2	9.7503	-0.2497
Ni	3	9.6226	-0.3774
Ni	4	9.6225	-0.3775
Ni	5	9.6887	-0.3113
Ni	6	9.6881	-0.3119
Ni	7	9.6867	-0.3133
Ni	8	9.6862	-0.3138
Ni	9	9.7507	-0.2493
Ni	10	9.7493	-0.2507
Ni	11	9.6229	-0.3771
Ni	12	9.6224	-0.3776
Ni	13	9.6883	-0.3117
Ni	14	9.6884	-0.3116
Ni	15	9.6863	-0.3137
Ni	16	9.686	-0.314

Ni	17	9.7495	-0.2505
Ni	18	9.7496	-0.2504
Ni	19	9.6227	-0.3773
Ni	20	9.6224	-0.3776
Ni	21	9.6886	-0.3114
Ni	22	9.6889	-0.3111
Ni	23	9.6862	-0.3138
Ni	24	9.6863	-0.3137
Ni	25	9.7502	-0.2498
Ni	26	9.7498	-0.2502
Ni	27	9.6227	-0.3773
Ni	28	9.6226	-0.3774
Ni	29	9.6885	-0.3115
Ni	30	9.6892	-0.3108
Ni	31	9.6868	-0.3132
Ni	32	9.6864	-0.3136
Ni	33	9.7497	-0.2503
Ni	34	9.7497	-0.2503
Ni	35	9.6222	-0.3778
Ni	36	9.6227	-0.3773
Ni	37	9.6886	-0.3114
Ni	38	9.6887	-0.3113
Ni	39	9.6868	-0.3132
Ni	40	9.6864	-0.3136
Ni	41	9.7496	-0.2504
Ni	42	9.7502	-0.2498
Ni	43	9.6225	-0.3775
Ni	44	9.6223	-0.3777
Ni	45	9.6884	-0.3116
Ni	46	9.6883	-0.3117
Ni	47	9.6863	-0.3137
Ni	48	9.686	-0.314
Se	49	6.3147	0.3147
Se	50	6.3145	0.3145
Se	51	6.2947	0.2947
Se	52	6.2949	0.2949
Se	53	6.3669	0.3669
Se	54	6.3666	0.3666
Se	55	6.2758	0.2758
Se	56	6.2761	0.2761
Se	57	6.3144	0.3144
Se	58	6.3155	0.3155
Se	59	6.2947	0.2947
Se	60	6.2948	0.2948
Se	61	6.3674	0.3674
Se	62	6.3679	0.3679
Se	63	6.2756	0.2756
Se	64	6.2764	0.2764
Se	65	6.3145	0.3145

Se	66	6.3151	0.3151
Se	67	6.295	0.295
Se	68	6.2954	0.2954
Se	69	6.3671	0.3671
Se	70	6.3672	0.3672
Se	71	6.2761	0.2761
Se	72	6.2755	0.2755
Se	73	6.315	0.315
Se	74	6.3155	0.3155
Se	75	6.2949	0.2949
Se	76	6.2942	0.2942
Se	77	6.3666	0.3666
Se	78	6.3667	0.3667
Se	79	6.2756	0.2756
Se	80	6.2757	0.2757
Se	81	6.3145	0.3145
Se	82	6.3151	0.3151
Se	83	6.2949	0.2949
Se	84	6.2948	0.2948
Se	85	6.3667	0.3667
Se	86	6.3664	0.3664
Se	87	6.2757	0.2757
Se	88	6.2759	0.2759
Se	89	6.315	0.315
Se	90	6.3158	0.3158
Se	91	6.295	0.295
Se	92	6.2948	0.2948
Se	93	6.3669	0.3669
Se	94	6.3673	0.3673
Se	95	6.2757	0.2757
Se	96	6.2758	0.2758

Table S5. Bader charge analysis of FeCo LDH.

Element	Atom number	Quantity of charge	Change of charges
		(e)	(e)
Fe	1	6.5693	-1.4307
Fe	2	6.5983	-1.4017
Fe	3	6.5885	-1.4115
Fe	4	6.7321	-1.2679
Fe	5	6.724	-1.276
Fe	6	6.5805	-1.4195
Fe	7	6.57	-1.43
Fe	8	6.7337	-1.2663
O	9	7.2511	1.2511
O	10	7.2398	1.2398
O	11	7.2636	1.2636
O	12	7.2256	1.2256
O	13	7.2241	1.2241

O	14	7.2346	1.2346
O	15	7.2211	1.2211
O	16	7.3137	1.3137
O	17	7.294	1.294
O	18	7.1764	1.1764
O	19	7.1452	1.1452
O	20	7.2877	1.2877
O	21	7.1791	1.1791
O	22	7.2017	1.2017
O	23	7.324	1.324
O	24	7.1519	1.1519
O	25	7.228	1.228
O	26	7.216	1.216
O	27	7.2337	1.2337
O	28	7.2151	1.2151
O	29	7.1979	1.1979
O	30	7.2157	1.2157
O	31	7.1552	1.1552
O	32	7.283	1.283
O	33	7.1755	1.1755
O	34	7.3151	1.3151
O	35	7.1467	1.1467
O	36	7.2626	1.2626
O	37	7.1939	1.1939
O	38	7.1723	1.1723
O	39	7.2538	1.2538
O	40	7.2161	1.2161
H	41	0.4093	-0.5907
H	42	0.4432	-0.5568
H	43	0.4107	-0.5893
H	44	0.4297	-0.5703
H	45	0.3826	-0.6174
H	46	0.3873	-0.6127
H	47	0.4324	-0.5676
H	48	0.3446	-0.6554
H	49	0.3849	-0.6151
H	50	0.4337	-0.5663
H	51	0.4498	-0.5502
H	52	0.3701	-0.6299
H	53	0.4371	-0.5629
H	54	0.4114	-0.5886
H	55	0.3471	-0.6529
H	56	0.4493	-0.5507
H	57	0.3786	-0.6214
H	58	0.4052	-0.5948
H	59	0.4394	-0.5606
H	60	0.3846	-0.6154
H	61	0.4136	-0.5864
H	62	0.4125	-0.5875

H	63	0.444	-0.556
H	64	0.3809	-0.6191
H	65	0.4462	-0.5538
H	66	0.3453	-0.6547
H	67	0.4496	-0.5504
H	68	0.3944	-0.6056
H	69	0.4239	-0.5761
H	70	0.442	-0.558
H	71	0.419	-0.581
H	72	0.3821	-0.6179
Co	73	7.8346	-1.1654
Co	74	7.8373	-1.1627
Co	75	7.8208	-1.1792
Co	76	7.8151	-1.1849
Co	77	7.8251	-1.1749
Co	78	7.8285	-1.1715
Co	79	7.8238	-1.1762
Co	80	7.8195	-1.1805

Table S6. Bader charge analysis of FeCo LDH/NiSe.

Element	Atom number	Quantity of charge	Change of charges
		(e)	(e)
Ni	1	9.7615	-0.2385
Ni	2	9.7646	-0.2354
Ni	3	9.6498	-0.3502
Ni	4	9.6543	-0.3457
Ni	5	9.7114	-0.2886
Ni	6	9.7191	-0.2809
Ni	7	9.7299	-0.2701
Ni	8	9.7347	-0.2653
Ni	9	9.7652	-0.2348
Ni	10	9.7649	-0.2351
Ni	11	9.6511	-0.3489
Ni	12	9.6497	-0.3503
Ni	13	9.7156	-0.2844
Ni	14	9.714	-0.286
Ni	15	9.7096	-0.2904
Ni	16	9.7112	-0.2888
Ni	17	9.7624	-0.2376
Ni	18	9.7641	-0.2359
Ni	19	9.6493	-0.3507
Ni	20	9.6539	-0.3461
Ni	21	9.7125	-0.2875
Ni	22	9.718	-0.282
Ni	23	9.7308	-0.2692
Ni	24	9.7357	-0.2643
Ni	25	9.7654	-0.2346
Ni	26	9.7644	-0.2356

Ni	27	9.65	-0.35
Ni	28	9.6499	-0.3501
Ni	29	9.7156	-0.2844
Ni	30	9.7144	-0.2856
Ni	31	9.7095	-0.2905
Ni	32	9.7098	-0.2902
Se	33	6.3188	0.3188
Se	34	6.3193	0.3193
Se	35	6.4002	0.4002
Se	36	6.4044	0.4044
Se	37	6.3427	0.3427
Se	38	6.3402	0.3402
Se	39	6.3331	0.3331
Se	40	6.3191	0.3191
Se	41	6.3153	0.3153
Se	42	6.3211	0.3211
Se	43	6.405	0.405
Se	44	6.3929	0.3929
Se	45	6.3492	0.3492
Se	46	6.3426	0.3426
Se	47	6.3396	0.3396
Se	48	6.3509	0.3509
Se	49	6.3178	0.3178
Se	50	6.3188	0.3188
Se	51	6.4007	0.4007
Se	52	6.405	0.405
Se	53	6.3413	0.3413
Se	54	6.341	0.341
Se	55	6.3353	0.3353
Se	56	6.319	0.319
Se	57	6.3146	0.3146
Se	58	6.3201	0.3201
Se	59	6.4056	0.4056
Se	60	6.3925	0.3925
Se	61	6.3488	0.3488
Se	62	6.3428	0.3428
Se	63	6.3402	0.3402
Se	64	6.351	0.351
Fe	65	6.498	-1.502
Fe	66	6.4805	-1.5195
Fe	67	6.5048	-1.4952
Fe	68	6.5116	-1.4884
Fe	69	6.4803	-1.5197
Fe	70	6.5065	-1.4935
Fe	71	6.4987	-1.5013
Fe	72	6.4808	-1.5192
Fe	73	6.5043	-1.4957
Fe	74	6.5102	-1.4898
Fe	75	6.4803	-1.5197

Fe	76	6.5063	-1.4937
O	77	7.3154	1.3154
O	78	7.2252	1.2252
O	79	7.2834	1.2834
O	80	7.2464	1.2464
O	81	7.2282	1.2282
O	82	7.2951	1.2951
O	83	7.2709	1.2709
O	84	7.2599	1.2599
O	85	7.292	1.292
O	86	7.2601	1.2601
O	87	7.3182	1.3182
O	88	7.2413	1.2413
O	89	7.2638	1.2638
O	90	7.2139	1.2139
O	91	7.291	1.291
O	92	7.2492	1.2492
O	93	7.2647	1.2647
O	94	7.2274	1.2274
O	95	7.2277	1.2277
O	96	7.3093	1.3093
O	97	7.3163	1.3163
O	98	7.2231	1.2231
O	99	7.2882	1.2882
O	100	7.2418	1.2418
O	101	7.2269	1.2269
O	102	7.2951	1.2951
O	103	7.2705	1.2705
O	104	7.2602	1.2602
O	105	7.2917	1.2917
O	106	7.2612	1.2612
O	107	7.3222	1.3222
O	108	7.2417	1.2417
O	109	7.2605	1.2605
O	110	7.2149	1.2149
O	111	7.2913	1.2913
O	112	7.247	1.247
O	113	7.2651	1.2651
O	114	7.2273	1.2273
O	115	7.2251	1.2251
O	116	7.2366	1.2366
H	117	0.3483	-0.6517
H	118	0.4162	-0.5838
H	119	0.3593	-0.6407
H	120	0.3892	-0.6108
H	121	0.4301	-0.5699
H	122	0.3316	-0.6684
H	123	0.3818	-0.6182
H	124	0.3679	-0.6321

H	125	0.3686	-0.6314
H	126	0.3852	-0.6148
H	127	0.3456	-0.6544
H	128	0.4037	-0.5963
H	129	0.3925	-0.6075
H	130	0.4085	-0.5915
H	131	0.3614	-0.6386
H	132	0.3933	-0.6067
H	133	0.3809	-0.6191
H	134	0.4013	-0.5987
H	135	0.428	-0.572
H	136	0.3469	-0.6531
H	137	0.3471	-0.6529
H	138	0.4183	-0.5817
H	139	0.3571	-0.6429
H	140	0.3927	-0.6073
H	141	0.4305	-0.5695
H	142	0.3322	-0.6678
H	143	0.3822	-0.6178
H	144	0.3678	-0.6322
H	145	0.3684	-0.6316
H	146	0.3845	-0.6155
H	147	0.3421	-0.6579
H	148	0.4031	-0.5969
H	149	0.3958	-0.6042
H	150	0.4078	-0.5922
H	151	0.3617	-0.6383
H	152	0.3957	-0.6043
H	153	0.3807	-0.6193
H	154	0.401	-0.599
H	155	0.4311	-0.5689
H	156	0.4207	-0.5793
Co	157	7.7772	-1.2228
Co	158	7.7734	-1.2266
Co	159	7.7702	-1.2298
Co	160	7.7721	-1.2279
Co	161	7.7779	-1.2221
Co	162	7.7739	-1.2261
Co	163	7.7694	-1.2306
Co	164	7.7717	-1.2283

References

1. L. Yu, H. Zhou, J. Sun, F. Qin, F. Yu, J. Bao, Y. Yu, S. Chen, Z. Ren, Cu nanowires shelled with NiFe layered double hydroxide nanosheets as bifunctional electrocatalysts for overall water splitting, *Energy Environ. Sci.*, 2017, **10**, 1820-1827.
2. H. Zhou, F. Yu, Q. Zhu, J. Sun, F. Qin, L. Yu, J. Bao, Y. Yu, S. Chen, Z. Ren, Water splitting by electrolysis at high current densities under 1.6 volts, *Energy Environ. Sci.*, 2018, **11**, 2858-2864.
3. Q. Wen, K. Yang, D. Huang, G. Cheng, X. Ai, Y. Liu, J. Fang, H. Li, L. Yu, T. Zhai, Schottky Heterojunction Nanosheet Array Achieving High-Current-Density Oxygen Evolution for Industrial Water Splitting Electrolyzers, *Adv. Energy Mater.*, 2021, **11**, 2102353.
4. J. Liu, W. Du, S. Guo, J. Pan, J. Hu, X. Xu, Iron-Locked Hydr(oxy)oxide Catalysts via Ion-Compensatory Reconstruction Boost Large-Current-Density Water Oxidation, *Adv. Sci.*, 2023, **10**, e2300717.
5. X. Cheng, Z. Pan, C. Lei, Y. Jin, B. Yang, Z. Li, X. Zhang, L. Lei, C. Yuan, Y. Hou, A strongly coupled 3D ternary $\text{Fe}_2\text{O}_3@\text{Ni}_2\text{P}/\text{Ni}(\text{PO}_3)_2$ hybrid for enhanced electrocatalytic oxygen evolution at ultra-high current densities, *J. Mater. Chem. A*, 2019, **7**, 965-971.
6. F. Yu, H. Zhou, Y. Huang, J. Sun, F. Qin, J. Bao, W.A. Goddard, S. Chen, Z. Ren, High-performance bifunctional porous non-noble metal phosphide catalyst for overall water splitting, *Nat. Commun.*, 2018, **9**, 2551.
7. X. Y. Zhang, F. T. Li, Y. W. Dong, B. Dong, F. N. Dai, C. G. Liu, Y. M. Chai, Dynamic anion regulation to construct S-doped FeOOH realizing 1000 mA cm⁻²-level-current-density oxygen evolution over 1000 h, *Appl. Catal. B: Environ.*, 2022, **315**, 121571.
8. G. Deng, J. Zhao, H. S. Hu, X. Y. Wang, M. Zhu, Y. Y. Feng, FeOOH-CoS composite catalyst with high catalytic performances for oxygen evolution reaction at high current density, *Int. J. Hydrogen Energy*, 2021, **46**, 37333-37339.
9. X. Zhang, H. Yi, M. Jin, Q. Lian, Y. Huang, Z. Ai, R. Huang, Z. Zuo, C. Tang, A. Amini, F. Jia, S. Song, C. Cheng, In Situ Reconstructed Zn doped $\text{Fe}_{(x)}\text{Ni}_{(1-x)}\text{OOH}$ Catalyst for Efficient and Ultrastable Oxygen Evolution Reaction at High Current Densities, *Small*, 2022, **18**, e2203710.
10. R. Andaveh, A. Sabour Rouhaghdam, J. Ai, M. Maleki, K. Wang, A. Seif, G. Barati Darband, J. Li, Boosting the electrocatalytic activity of NiSe by introducing MnCo as an efficient heterostructured electrocatalyst for large-current-density alkaline seawater splitting, *Appl. Catal. B: Environ.*, 2023, **325**, 122355.
11. Q. N. Bian, B. S. Guo, D. X. Tan, D. Zhang, W. Q. Kong, C. B. Wang, Y. Y. Feng, Constructing CoNi-LDH/Fe MOF/NF Heterostructure Catalyst for Energy-Efficient OER and UOR at High Current Density, *ACS Appl. Mater. Interfaces*, 2024, **16**, 14742-14749.
12. G. Qian, J. Chen, T. Yu, J. Liu, L. Luo, S. Yin, Three-Phase Heterojunction NiMo-Based Nano-Needle for Water Splitting at Industrial Alkaline Condition, *Nanomicro. Lett.*, 2021, **14**, 20.

13. G. Qian, J. Chen, T. Yu, L. Luo, S. Yin, N-Doped Graphene-Decorated NiCo Alloy Coupled with Mesoporous NiCoMoO Nano-sheet Heterojunction for Enhanced Water Electrolysis Activity at High Current Density, *Nanomicro. Lett.*, 2021, **13**, 77.
14. X. Y. Wang, M. Zhu, Q. N. Bian, B. S. Guo, W. Q. Kong, C. B. Wang, Y. Y. Feng, Fe-Based Metal–Organic Framework-Ni₃S₂ Heterostructure Nanocomposites for Efficient Oxygen Evolution Reaction at High Current Densities, *ACS Appl. Nano Mater.*, 2023, **6**, 5200-5210.
15. Y. Qian, F. Zhang, L. Qiu, W. Han, Z. Zeng, L. Lei, Y. He, P. Li, X. Zhang, Optimizing electronic structure of NiFe LDH with Mn-doping and Fe_{0.64}Ni_{0.36} alloy for alkaline water oxidation under industrial current density, *Nano Res.*, 2023, **16**, 8953-8960.
16. X. Mu, X. Gu, S. Dai, J. Chen, Y. Cui, Q. Chen, M. Yu, C. Chen, S. Liu, S. Mu, Breaking the symmetry of single-atom catalysts enables an extremely low energy barrier and high stability for large-current-density water splitting, *Energy Environ. Sci.*, 2022, **1**, 4048-4057.
17. L. Wu, L. Yu, F. Zhang, B. McElhenny, D. Luo, A. Karim, S. Chen, Z. Ren, Heterogeneous Bimetallic Phosphide Ni₂P-Fe₂P as an Efficient Bifunctional Catalyst for Water/Seawater Splitting, *Adv. Funct. Mater.*, 2020, **31**, 2006484.
18. S. Niu, W. J. Jiang, Z. Wei, T. Tang, J. Ma, J. S. Hu and L. J. Wan, Se-Doping Activates FeOOH for Cost-Effective and Efficient Electrochemical Water Oxidation, *J. Am. Chem. Soc.*, 2019, **141**, 7005-7013.
19. X. Cheng, Z. Pan, C. Lei, Y. Jin, B. Yang, Z. Li, X. Zhang, L. Lei, C. Yuan and Y. Hou, A strongly coupled 3D ternary Fe₂O₃@Ni₂P/Ni(PO₃)₂ hybrid for enhanced electrocatalytic oxygen evolution at ultra-high current densities, *J. Mater. Chem. A*, 2019, **7**, 965-971.
20. X. Luo, P. Ji, P. Wang, R. Cheng, D. Chen, C. Lin, J. Zhang, J. He, Z. Shi, N. Li, S. Xiao and S. Mu, Interface Engineering of Hierarchical Branched Mo-Doped Ni₃S₂/Ni_xP_y Hollow Heterostructure Nanorods for Efficient Overall Water Splitting, *Adv. Energy Mater.*, 2020, **10**, 1903891.
21. J. Li, Z. Yuan, Y. Zhu, D. Li, W. Han, L. Li and G. Li, Engineering multiphasic heterostructure NiCoP@Co_{0.5}Ni_{0.5}Se₂ with optimized electronic structure enabling robust hydrogen evolution, *Chem. Eng. J.*, 2022, **450**, 138426.
22. Z. Zou, X. Wang, J. Huang, Z. Wu and F. Gao, An Fe-doped nickel selenide nanorod/nanosheet hierarchical array for efficient overall water splitting, *J. Mater. Chem. A*, 2019, **7**, 2233-2241.
23. L. Ji, J. Wang, X. Teng, T. J. Meyer and Z. Chen, CoP Nanoframes as Bifunctional Electrocatalysts for Efficient Overall Water Splitting, *ACS Catal.*, 2019, **10**, 412-419.
24. H. Fan, D. Jiao, J. Fan, D. Wang, B. Zaman, W. Zhang, L. Zhang, W. Zheng and X. Cui, Kinetically and thermodynamically expediting elementary steps via high-valence Cr-incorporated of nickel selenide for water electrolysis, *Nano Res.*, 2023, **17**, 1199-1208.
25. W. Y. Fu, Y. X. Lin, M. S. Wang, S. Si, L. Wei, X. S. Zhao and Y. S. Wei,

- Sepaktakraw-like catalyst Mn-doped CoP enabling ultrastable electrocatalytic oxygen evolution at $100 \text{ mA}\cdot\text{cm}^{-2}$ in alkali media, *Rare Metals*, 2022, **41**, 3069-3077.
- 26. Y. Luo, P. Wang, S. Wu, G. Zhang, S. Sun, H. Ranganathan and Z. Shi, Simultaneous heterostructure engineering and Mn doping modulation of Ni_2P nanosheet arrays for enhanced electrocatalytic water splitting, *Sci. China Mater.*, 2022, **65**, 1814-1824.
 - 27. X. Shan, J. Liu, H. Mu, Y. Xiao, B. Mei, W. Liu, G. Lin, Z. Jiang, L. Wen and L. Jiang, An Engineered Superhydrophilic/Superaerophobic Electrocatalyst Composed of the Supported CoMoS_x Chalcogel for Overall Water Splitting, *Angew. Chem. Int. Ed.*, 2020, **59**, 1659-1665.